



# Design and development of a compliant piezoelectric microgripper based on three-stage amplification

Lei Ni<sup>1,2</sup> · Guoqiang Chen<sup>3</sup> · Kunpeng Hong<sup>3</sup> · Geng Wang<sup>1,2,3</sup>

Received: 25 June 2022 / Accepted: 7 June 2023 / Published online: 17 June 2023  
© The Author(s), under exclusive licence to Springer-Verlag GmbH Germany, part of Springer Nature 2023

## Abstract

This work presented the design and test of a double-arm actuated compliant piezoelectric microgripper based on three-stage amplification mechanism, which can also perceive the gripping displacement and force simultaneously. Developing a proper structure for the microgripper to achieve large amplification ratio in a compact space and to ensure sufficient natural frequency is a fundamental and challenging task. Firstly, the structure of piezoelectric microgripper was designed and the kinematic principle of the amplification mechanism was analyzed. Meanwhile, theoretical and simulation analysis of the statics and dynamics were carried out. Then, the calibration methods for both force and displacement sensors are presented. The calibration coefficients are 0.163 mN/mV and 0.040  $\mu\text{m}/\text{mV}$ , respectively. Finally, a series of experiments were performed to verify the performance of the designed microgripper. The test results show that the displacement amplification ratio of the microgripper is 16.8, and the maximum output displacement of 102.30  $\mu\text{m}$  and the maximum gripping force of 227.70 mN can be reached when applying a sinusoidal input voltage with the frequency of 0.10 Hz and the amplitude of 100 V. The closed-loop experiment shows that the peak-to-valley errors of both gripping displacement and force are less than 0.49  $\mu\text{m}$  and 3.74 mN respectively. The obtained natural frequency of 215.1 Hz. The micro-gripper achieves excellent static and dynamic performance in clamping accuracy, natural frequency, clamping range, and dual finger independence.

## 1 Introduction

As the end-effector of micro-assembly systems (Wang et al. 2021a), the performance of a microgripper (Fard-Vatan and Hamedi 2020) (Chen et al. 2017) often greatly affects the success or failure of the assembly task because it directly contacts the manipulated object during the assembly operation (Lyu and Qingsong 2021). How to accurately grip, carry and release the operated object is the key point to the micro-assembly task (Chang et al. 2020) (Wang et al. 2021b). In the process of gripping, it is

necessary to accurately detect and control the finger displacement and force of the microgripper so as to avoid excessive gripping force damaging the operated object or too small gripping force causing the operated object to fall off in the process of gripping. Therefore, it is of great practical significance (Zhang et al. 2018) (Liang et al. 2018) to design a microgripper with sound structural characteristics, large gripping range, and the ability to accurately detect and control the finger displacement and gripping force of the microgripper to promote the development of micro-assembly and micro-manipulation technology and micro-electro-mechanical system (Ding et al. 2019).

The piezoelectric microgripper takes advantage of the inverse piezoelectric effect (Han et al. 2015) of piezoelectric ceramics to realize the gripping and releasing operation. Due to the advantages (Aabid et al. 2021) of fast response, high resolution and large driving force of piezoelectric ceramics, microgripper driven by piezoelectric actuator is the most widely used (Wang et al. 2021c; Zheng and Weijie 2022). By using the lever mechanism and parallel quadrilateral mechanism to amplify and

✉ Geng Wang  
wgmouse@163.com

<sup>1</sup> Key Laboratory of Testing Technology for Manufacturing Process of Ministry of Education, Southwest University of Science and Technology, Mianyang 621010, China

<sup>2</sup> Tianfu Institute of Research and Innovation, Southwest University of Science and Technology, Chengdu 610299, China

<sup>3</sup> School of Mechanical and Power Engineering, Henan Polytechnic University, Jiaozuo 454000, China

transfer the displacement, Nah and Zhong (2007) developed a piezoelectric microgripper which can grip the metal wire with a diameter of 500  $\mu\text{m}$ . And the achieved amplification ratio is 3 and the maximum gripping range is 170  $\mu\text{m}$ . Zubir et al. (2009) developed an asymmetric piezoelectric microgripper with an overall size of 50 mm  $\times$  30 mm, which is made of advanced aluminum alloy and processed by precision wire cutting technology. The test results show that the actual amplification ratio of the designed microgripper is 3.8, and the maximum output displacement of the finger tip is 100  $\mu\text{m}$ . Several research works (Liang et al. 2017; Koo et al. 2015) have been reported on the mechanical design of microgrippers with different specifications. However, the sensing of gripping force and displacement is another important aspect to improve the gripping performance.

Due to the existence of hysteresis nonlinearity (Wang and Rao 2015; Ren et al. 2020) of piezoelectric materials, it is necessary to control or compensate for the nonlinear characteristic based on different sensing methods when it is used in high-precision gripping operation. Yuguo and Yaoxiang (2015) developed a piezoelectric microgripper based on a flexible lever amplification mechanism, which uses a resistive strain gauge to measure the finger displacement and gripping force. This microgripper has the advantages of compact structure, translatable finger and high gripping sensitivity. Yang et al. (2015) developed a compliant piezoelectric microgripper with integrated displacement and force sensors by using a bridge amplification mechanism. The microgripper is driven by two driving power supplies, and it can synchronously control the finger displacement and gripping force. Wang et al. (2013) developed a monolithic compliant piezoelectric microgripper by using compliant parallelogram mechanism and lever amplification mechanism to transfer and amplify displacement. The displacement and force sensors integrated can detect the output displacement and gripping force. Although the above designed a piezoelectric microgripper and obtained a large displacement amplification ratio, the dynamic characteristics of the microgripper have not been presented.

In order to improve the efficiency, quality and cost of micromanipulation and assembly, and realize the simultaneous sensing of gripping force and displacement, this paper presents the structure design, modeling analysis, optimization, manufacturing and experimental testing of a new piezoelectric actuated microgripper with a three-stage compliant amplification mechanism. Different from the existing works (Chen et al. 2019), the feature of this paper is to design a compact piezoelectric microgripper with simple mechanism, low cost, high precision and perceptive force/displacement, which can be used for accurate detection and control of finger displacement and gripping force.

## 2 Mechanism of the microgripper

Figure 1 shows the mechanism of the proposed symmetrical double-arm compliant piezoelectric microgripper based on a three-stage displacement amplification. The microgripper consists of PZT actuators, strain displacement sensor, strain force sensor, preloaded bolts, gasket and base. Wherein,  $A_1$ ,  $A_2$ ,  $A_3$ ,  $A_4$ ,  $C$ ,  $D_1$ ,  $D_2$  are single-notch right circular flexure hinges which are very precise in keeping the positions of the rotation centers (Zhang and Hu 2009),  $E$  and  $F$  are double-notch right circular flexure hinges (Yong et al. 2008), and  $B$  is a rectangular flexure hinge. The microgripper adopts a symmetrical structure configuration, where two piezoelectric actuators are installed symmetrically inside to make full use of the space. The three-stage amplification mechanism consists of the first-stage lever amplification mechanism ( $F$ - $E$ - $D_1$ ), the second-stage triangle amplification mechanism ( $D_1$ - $C$ - $D_2$ ), and the third-stage lever amplification mechanism ( $A_3$ - $B$ - $A_2$ ). In addition, the parallelogram mechanism ( $A_1$ - $A_2$ - $A_3$ - $A_4$ ) can ensure complete translational motion of the gripping action.

The motion transmission of the microgripper is carried out as follows. Under the action of driving voltage, the left piezoelectric actuator produces an input displacement to push the linkage  $D_1$ - $F$  to rotate clockwise around the hinge  $F$ , thus driving the linkage  $D_1$ - $C$  to make the hinge  $C$  move clockwise around  $D_2$ . linkage  $BC$  moves to the right and drives linkage  $A_2$ - $A_3$  to move clockwise around the hinge  $A_3$  through hinge  $B$ . Because  $A_1$ - $A_2$ - $A_3$ - $A_4$  is a parallelogram mechanism, linkage  $A_1$ - $A_2$  can achieve translational movement to the right, while the symmetrical right

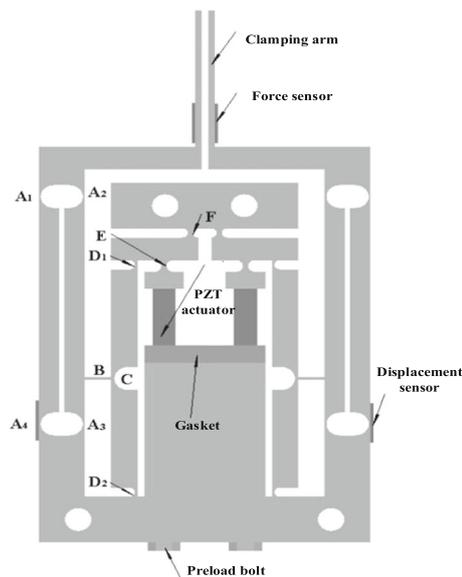


Fig. 1 Mechanism of the proposed microgripper

structure will translational to the left. And then the relative movement of the left and right clamping arms will achieve the gripping action of the object. When the power is switched to OFF, the piezoelectric actuator shrinks to its initial position, causing the clamping arm to open and release the object being manipulated. The displacement sensor is pasted on the outside of the flexible hinge A4 to detect the output displacement, and the force sensor is pasted on the root of the clamping arm to detect the gripping force. The microgripper has the advantages of small size, simple structure, large gripping range and translational gripping.

### 3 Modeling, optimization, and analysis

#### 3.1 Kinematic principle

It is assumed that the elastic deformation of the microgripper only occurs at the flexure hinge, and other parts are regarded as rigid bodies. In addition, the flexure hinge can only bend and the rotation angle is very small without any expansions or contractions. According to the pseudo-rigid body theory, the flexible three-stage amplification mechanism of microgripper designed in this paper can be regarded as a rotating pair connecting two rigid bodies, as shown in Fig. 2, where  $\varphi_1, \varphi_2, \varphi_3, \varphi_4, \varphi_5$  is the initial angle of the linkages AB, BC, BE, FE and DC,  $\alpha$  and  $\beta$  are the angles between AF and AD and the positive direction of  $x$  axis respectively, and  $d_{in}$  and  $d_{out}$  are the input and output displacements respectively.

The mechanism of the three-stage amplification microgripper can be decomposed into two closed planar four-bar linkage mechanisms, namely, A–B–C–D and A–B–E–F. The position equations of the two four-bar linkage mechanisms can be established by using the vector method:

$$\vec{AB} + \vec{BC} - \vec{DC} - \vec{AD} = 0 \tag{1}$$

$$\vec{AB} + \vec{BE} - \vec{FE} - \vec{AF} = 0 \tag{2}$$

Rewrite equations (1) and (2) in the plural form as follows:

$$l_{AB}e^{i\varphi_1} + l_{BC}e^{i\varphi_2} = l_{CD}e^{i\varphi_5} + l_{AD}e^{i\beta} \tag{3}$$

$$l_{AB}e^{i\varphi_1} + l_{BE}e^{i\varphi_3} = l_{AF}e^{i\alpha} + l_{FE}e^{i\varphi_4} \tag{4}$$

where,  $l_{AB}, l_{BC}, l_{CD}, l_{AD}, l_{BE}, l_{AF}, l_{FE}$  represents the length of the linkages AB, BC, CD, AD, BE, AF and FE, respectively.

Based on Euler’s formula, let the real and imaginary parts of (3)–(4) are equal, and then the following expressions can be obtained:

$$l_{AB} \cos \varphi_1 + l_{BC} \cos \varphi_2 = l_{CD} \cos \varphi_5 + l_{AD} \cos \beta \tag{5}$$

$$l_{AB} \sin \varphi_1 + l_{BC} \sin \varphi_2 = l_{CD} \sin \varphi_5 + l_{AD} \sin \beta \tag{6}$$

$$l_{AB} \cos \varphi_1 + l_{BE} \cos \varphi_3 = l_{AF} \cos \alpha + l_{FE} \cos \varphi_4 \tag{7}$$

$$l_{AB} \sin \varphi_1 + l_{BE} \sin \varphi_3 = l_{AF} \sin \alpha + l_{FE} \sin \varphi_4 \tag{8}$$

Differentiating the four formulas from (5) to (8) with respect to time, and the following relationship can be achieved:

$$Aw = Bw_5 \tag{9}$$

where,  $A =$

$$A = \begin{bmatrix} l_{AB} \sin \varphi_1 & l_{BC} \sin \varphi_2 & 0 & 0 \\ l_{AB} \cos \varphi_1 & l_{BC} \cos \varphi_2 & 0 & 0 \\ l_{AB} \sin \varphi_1 & 0 & l_{BE} \sin \varphi_3 & -l_{FE} \sin \varphi_4 \\ l_{AB} \cos \varphi_1 & 0 & l_{BE} \cos \varphi_3 & -l_{FE} \cos \varphi_4 \end{bmatrix},$$

$$\omega = \begin{bmatrix} \omega_1 \\ \omega_2 \\ \omega_3 \\ \omega_4 \end{bmatrix}, B = \begin{bmatrix} l_{CD} \sin \varphi_5 \\ l_{CD} \cos \varphi_5 \\ 0 \\ 0 \end{bmatrix}$$

And then the displacement amplification ratio  $\lambda$  of the microgripper can be obtained as follows:

$$\lambda = \frac{d_{out}}{d_{in}} \approx \frac{\omega_4 l_{FI}}{\omega_5 l_{in}} = A^{-1}B(4, 1) \frac{l_{FI}}{l_{in}} \tag{10}$$

$$= \frac{l_{CD}l_{FI} \sin(\varphi_2 + \varphi_3) \sin(\varphi_2 - \varphi_5)}{2l_{FE}l_{in} \sin \varphi_2 \cos \varphi_2 \sin(\varphi_3 - \varphi_4)}$$

where,  $l_{FI}$  is the length of the linkage FI, and  $l_{in}$  is the distance from the input to the flexure hinge D.

By substituting the dimension parameters of the microgripper into formula (10), the theoretical amplification ratio of the microgripper can be obtained as 23.0. In

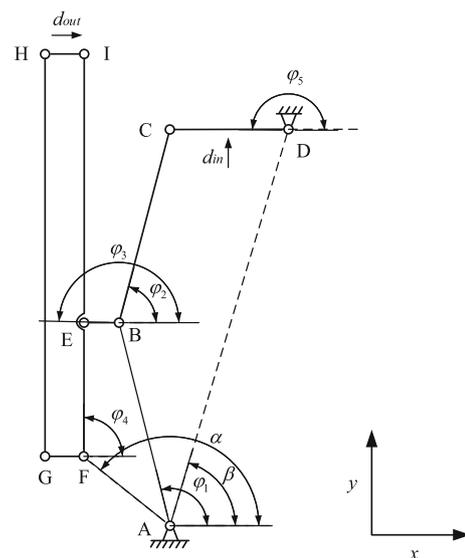


Fig. 2 Pseudo-rigid-body model of the three-stage amplification

this calculation, each connecting part of the microgripper is regarded as a rigid body, and only the geometric motion relationship is analyzed without considering the material properties. Therefore, this is a preliminary estimation of the amplification ratio, which will be furtherly calculated by finite element analysis (FEA) and experimental test respectively.

### 3.2 Static modeling

In this subsection, the pseudo-rigid-body-model (PRBM) method is used to establish the static model to describe the force–deflection relationship of flexible hinges and then the input stiffness of the microgripper can be obtained. By replacing the flexible segments with an equivalent rigid joint and a torsional spring, the microgripper can be regarded as a rigid body mechanism. This method is helpful to further study the performance of the microgripper to obtain some key design parameters.

When a small input displacement from the piezoelectric actuator is applied to the input end of the microgripper, the relevant rotational angle of the flexure hinges from A to I can be calculated as follows:

$$\phi_A = |\eta_1| \frac{d_{in}}{l_{in}} \tag{11}$$

$$\phi_B = |\eta_1 - \eta_2| \frac{d_{in}}{l_{in}} \tag{12}$$

$$\phi_C = |\eta_2 - 1| \frac{d_{in}}{l_{in}} \tag{13}$$

$$\phi_D = \frac{d_{in}}{l_{in}} \tag{14}$$

$$\phi_E = |\eta_2 - \eta_3| \frac{d_{in}}{l_{in}} \tag{15}$$

$$\phi_F = \phi_G = \phi_H = \phi_I = |\eta_4| \frac{d_{in}}{l_{in}} \tag{16}$$

where,  $\eta_1 = A^{-1}B(1, 1), \eta_2 = A^{-1}B(2, 1), \eta_3 = A^{-1}B(3, 1), \eta_4 = A^{-1}B(4, 1).$

According to literature (Awatar 2013; Paros and Weisbord 1965), the rotational stiffness of various flexure hinges can be estimated by the following formula:

$$K_i = \frac{\sqrt{2}Ebt_i^{5/2}}{9\pi r_i^{1/2}} \quad i = A, B, C, F, \dots I \tag{17}$$

$$K_D = \frac{2Ebt_D^{5/2}}{9\pi r_D^{1/2}} \tag{18}$$

$$K_E = \gamma_\theta K_\odot \frac{Ebd^3}{12l} \tag{19}$$

where,  $r_i$  and  $t_i$  are the radius and thickness of the relevant flexure hinge, respectively,  $E$  is the elastic modulus of the used material, and  $b$  and  $d$  are the thickness and width respectively,  $\gamma_\theta$  is the characteristic radius coefficient of the relevant flexure hinge,  $K_\odot$  is the stiffness coefficient of flexure hinge,  $l$  is the length of the relevant flexure hinge.

According to Castigliano’s first theory (Oden et al. 1982), the input force  $F_{in}$  that comes from the piezoelectric actuator and acts on end of the microgripper can be expressed as:

$$F_{in} = \frac{\partial U}{\partial d_{in}} \tag{20}$$

where,  $U$  is the elastic deformation potential energy, and can be expressed as

$$U = \frac{1}{2} \sum_{i=A}^I K_i \phi_i^2 \tag{21}$$

Substituting (11)–(19) into (21) yields

$$U = \frac{K_A \eta_1^2}{2l_{in}^2} d_{in}^2 + \frac{K_B (\eta_1 - \eta_2)^2}{2l_{in}^2} d_{in}^2 + \frac{K_C (\eta_1 - 1)^2}{2l_{in}^2} d_{in}^2 + \frac{K_D}{2l_{in}^2} d_{in}^2 + \frac{K_E (\eta_2 - \eta_3)^2}{2l_{in}^2} d_{in}^2 + \frac{4K_F \eta_4^2}{2l_{in}^2} d_{in}^2 \tag{22}$$

Then the input  $F_{in}$  force can be expressed as:

$$F_{in} = \frac{\partial U}{\partial d_{in}} = \left( \frac{K_A \eta_1^2}{l_{in}^2} + \frac{K_B (\eta_1 - \eta_2)^2}{l_{in}^2} + \frac{K_C (\eta_1 - 1)^2}{l_{in}^2} + \frac{K_D}{l_{in}^2} + \frac{K_E (\eta_2 - \eta_3)^2}{l_{in}^2} + \frac{4K_F \eta_4^2}{l_{in}^2} \right) d_{in} \tag{23}$$

Then input stiffness of the microgripper can be obtained as

$$K_{in} = \frac{K_A \eta_1^2}{l_{in}^2} + \frac{K_B (\eta_1 - \eta_2)^2}{l_{in}^2} + \frac{K_C (\eta_1 - 1)^2}{l_{in}^2} + \frac{K_D}{l_{in}^2} + \frac{K_E (\eta_2 - \eta_3)^2}{l_{in}^2} + \frac{4K_F \eta_4^2}{l_{in}^2} \tag{24}$$

From (24), we can see that the input stiffness of the designed microgripper is related to its geometric parameters.

### 3.3 Dynamic modeling

In this subsection, the Lagrange’s equation is used to establish the dynamic characteristics of the microgripper. The Lagrange’s equation can be expressed as follows:

$$\frac{d}{dt} \left( \frac{\partial T}{\partial \dot{q}_j} \right) - \frac{\partial T}{\partial q_j} + \frac{\partial V}{\partial q_j} = F_{Q_j} \quad j = 1, 2, \dots, N \quad (25)$$

where,  $T$  and  $V$  respectively denote the total kinetic energy and potential energy of the entire system,  $q_j$  represents the generalized coordinate of the system,  $\dot{q}_j$  represents the generalized velocity of the system,  $F_{Q_j}$  represents the generalized nonconservative force of the  $j$ th generalized coordinate of the system,  $N$  is the number of generalized coordinates.

The kinetic energy of the microgripper can be expressed as:

$$T = \frac{1}{2} J_{AB} \omega_1^2 + \frac{1}{2} J_{BC} \omega_2^2 + \frac{1}{2} J_{CD} \omega_3^2 + \frac{1}{2} J_{BE} \omega_4^2 + \frac{1}{2} (J_{FI} + J_{GH}) \omega_4^2 + \frac{1}{2} m_{out} \dot{d}_{out}^2 \quad (26)$$

where,  $J_{AB}$ ,  $J_{BC}$ ,  $J_{CD}$ ,  $J_{BE}$ ,  $J_{FI}$  and  $J_{GH}$  respectively represent the moment of inertia of the linkages AB, BC, CD, BE, FI and GH, and  $m_{out}$  represents the mass of the output end.

The potential energy of the microgripper can be expressed as:

$$V = \frac{1}{2} K_A \phi_A^2 + \frac{1}{2} K_B \phi_B^2 + \frac{1}{2} K_C \phi_C^2 + \frac{1}{2} K_D \phi_D^2 + \frac{1}{2} K_E \phi_E^2 + \frac{1}{2} \sum_{i=F}^I K_i \phi_i^2 \quad (27)$$

Substitute Equations (26) and (27) into Equations (25), then the dynamic model of the designed microgripper can be expressed as:

$$M' \ddot{\phi}_5 + K' \phi_5 = l_{in} F_{in} - \eta_4 l_{FI} F_{out} \quad (28)$$

where,  $F_{out}$  denotes the output force of the microgripper,  $M'$  and  $K'$  respectively represent the equivalent mass and equivalent stiffness of the microgripper, and can be expressed as:

$$K' = K_A \eta_1^2 + K_B (\eta_1 - \eta_2)^2 + K_C (\eta_1 - 1)^2 + K_D + K_E (\eta_2 - \eta_3)^2 + 4K_F \eta_4^2 \quad (29)$$

$$M' = J_{AB} \eta_1^2 + J_{BC} \eta_2^2 + J_{CD} + J_{BE} \eta_3^2 + 2J_{FI} \eta_4^2 + m_{out} l_{FI}^2 \eta_4^2 \quad (30)$$

Therefore, the working mode frequency of the microgripper can be obtained:

$$f_n = \frac{1}{2\pi} \sqrt{\frac{K'}{M'}} \quad (31)$$

Finally, the natural frequency of 243.5 Hz is calculated using the above formula and the designed parameters. This

result is on the basis of simplified analysis and needs to be verified by finite element method and experimental test.

### 3.4 Optimization design

In order to obtain an optimal microgripper structure, the following constraints and influencing factors (i–v) must be considered.

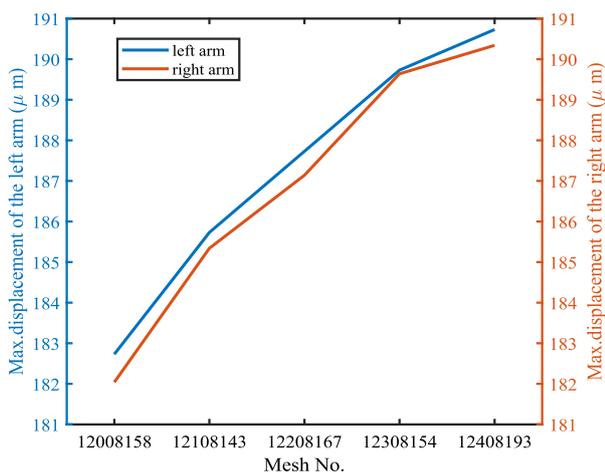
- (i) The key dimensional parameters that affect the performance of the microgripper are limited within a certain range.
- (ii) Input stiffness of the microgripper is limited by PZT stiffness.
- (iii) The equivalent stress of the critical part of the microgripper is limited by the yield strength of the material used.
- (iv) The natural frequency affects the speed performance of the microgripper.
- (v) Other manufacturing and safety factors.

In this work, the optimization objective of the design is to maximize the amplification ratio and the output displacement. In addition, during the optimization process it is necessary to ensure that the strain at the strain gauge sticking is large enough, and the overall structure of the microgripper should be compact. Finally, the designed parameters of the microgripper can be found by stochastic search optimization (Wang et al. 2015) based on the Ansys parametric design language programming.

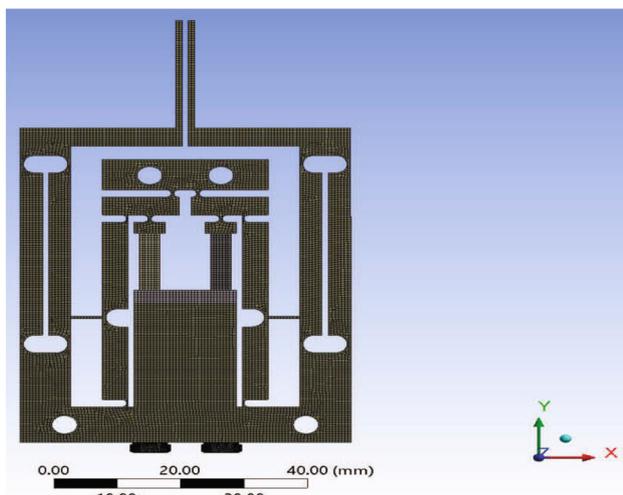
### 3.5 Characteristic analysis

This section will conduct the characteristic analysis of the optimized microgripper using the Ansys finite element software, including statics-based amplification ratio analysis and dynamics-based natural frequency analysis. These results can provide a quick insight into the performance evaluation of the microgripper.

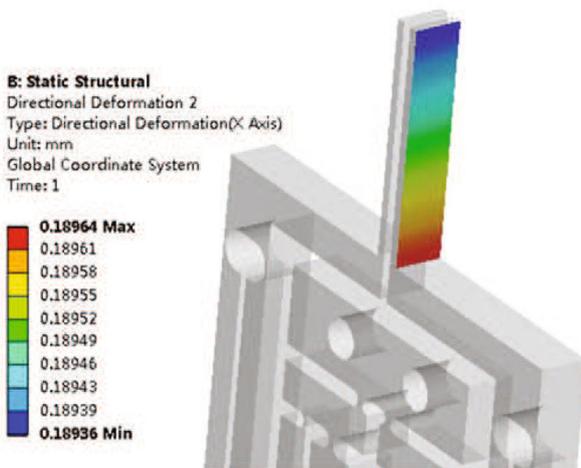
In general, the results of a static FEA analysis on the mechanism have high precision and confidence level compared to other types of finite element analyses (Jalili et al. 2022a). Nevertheless, we still need to analyze the influence (Jalili et al. 2022b, c) of the mesh at the location of the strain gauges. By using 5 different mesh numbers (12,008,158, 12108143, 12208167, 12308154, 12408193), we conducted a grid independence test. The obtained results are shown in Fig. 3a in the revised manuscript. It can be seen that with different grid densities, the results of strain distribution where the strain gauges are pasted have little difference, all of which are less than 1%. Given the small size of the model and the short computation time, a relatively fine meshing was chosen to obtain accurate results. In order to calculate the final model, the grid



(a) The diagram of grid independence



(b) The mesh diagram



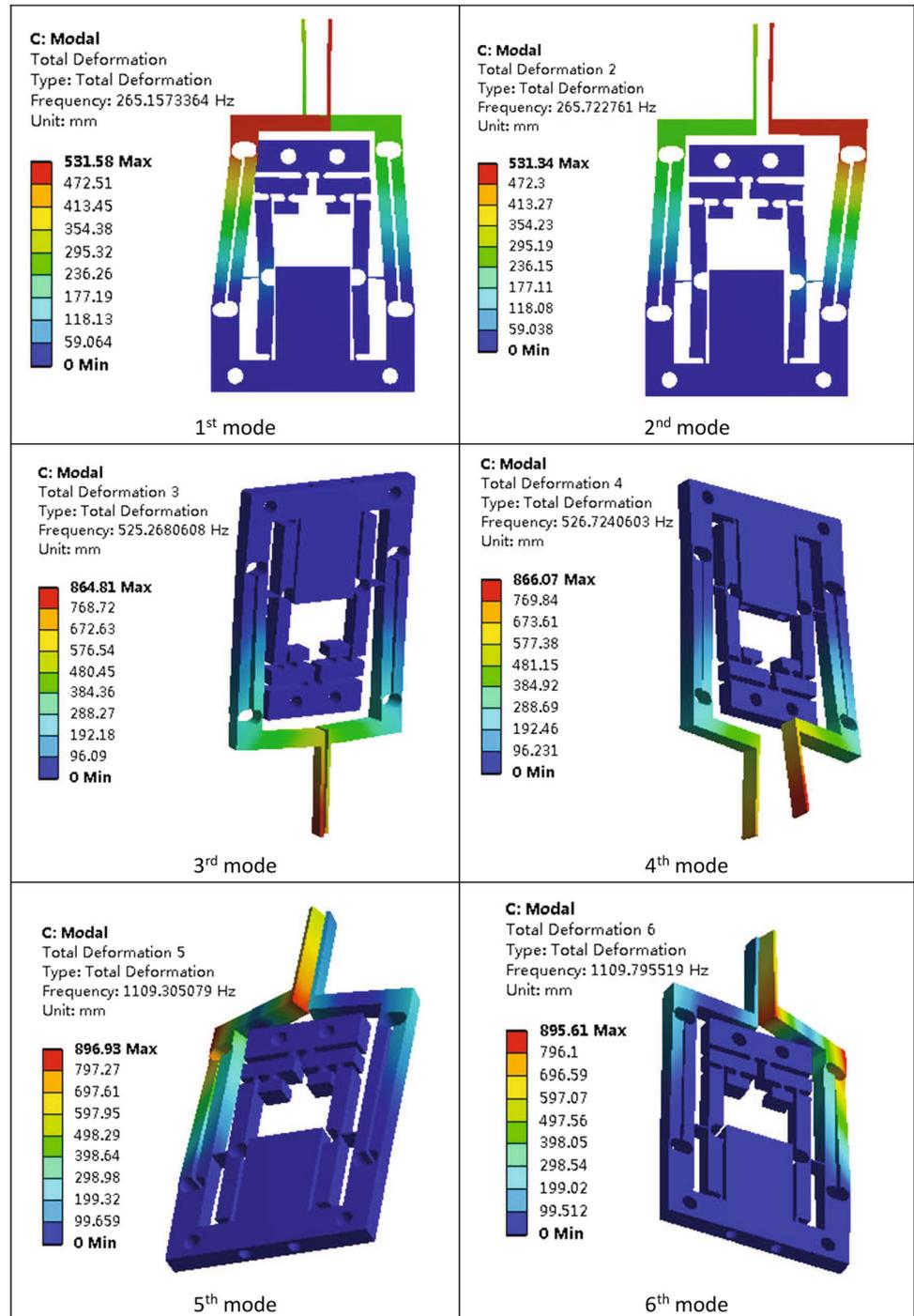
(c) Output displacement diagram of the right arm

Fig. 3 The static FEA analysis

system of 12308154 was chosen and the specific mesh diagram are added in Fig. 3b. In order to accurately analyze the displacement amplification ratio of the microgripper, an input displacement of 10  $\mu\text{m}$  is applied to the microgripper and the obtained maximum output displacement of the left arm is 189.73  $\mu\text{m}$ , and the maximum output displacement of the right arm is 189.64  $\mu\text{m}$ . The output displacements of the two arms are basically the same. It is reasonable to think that the displacement amplification ratio of the microgripper is 19.0. This value of ratio obtained by FEA is smaller than the theoretical value of 23.0, because the displacement loss arising from the bending and stretching will cause the actual amplification ratio to be smaller than the ideal one. The maximum stress of the microgripper is concentrated at the rectangular flexure hinge *B*, which is 81.5 Mpa, far less than the yield strength of 503 MPa, so the microgripper will not yield failure in the actual use. Furthermore, Fig. 3c presents the output displacement diagram of the arm of the microgripper. As can be seen from the figure, the output displacement of the arm gradually increases from top to bottom. The maximum output displacement is 189.64  $\mu\text{m}$  at the root of the clamping arm, and the minimum output displacement is 189.36  $\mu\text{m}$  at the top of the clamping arm. Only 0.28  $\mu\text{m}$  translational error is generated in the whole clamping arm, indicating that the designed microgripper has good translational performance and can achieve translational gripping of the operating object.

To verify the dynamic performance predicted by formula (31), Ansys-based modal analysis was conducted as shown in Fig. 4. The relevant properties of 7075 aluminum alloy material are density of 2.81  $\text{g}/\text{cm}^3$ , Modulus of 71.7 GPa and yield tensile strength of 503 MPa. The mesh model is established by 20-node element SOLID186. The natural frequencies of the first 6 orders obtained are 265.2 Hz, 265.7 Hz, 525.3 Hz, 526.7 Hz, 1109.3 Hz and 1109.8 Hz respectively. The frequencies of the first and second order are basically the same, indicating that the parallelogram mechanism drives the two clamping arms to move in reverse and in the same direction in the plane of the microgripper respectively. The frequencies of the third and fourth order are basically the same, representing the same and reverse torsional motion of the two clamping arms respectively. The frequencies of the fifth and sixth orders are basically the same, indicating the reverse torsional motion of the two clamping arms. Compared with the analytical calculation result (31), the deviation of the calculation result of the first order natural frequency is about 8%, which is caused by the simplified treatment in theoretical analysis.

**Fig. 4** The first 6 modes and natural frequencies



## 4 Preliminary tests

### 4.1 Prototype manufacturing and experimental setup

Figure 5 shows the prototype of the designed microgripper, which was fabricated by wire EDM to ensure the required

accuracy and was made from AL7075 with highly elastic, high yield strength, and light mass. In this work, the body of the microgripper is made of aluminum alloy AL7075, which is processed by Wire EDM (Electric Discharge Machining) technology. Nowadays, this is a relatively mature manufacturing process. In order to ensure the function of flexible deformation, PSA should be fully pre-

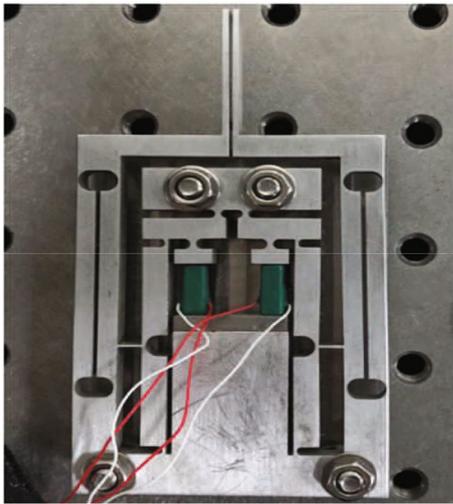


**Fig. 5** Prototype of the developed microgripper

tightened during assembly. The challenge of this work is how to design a proper structure for the microgripper to achieve large amplification ratio for displacement and force in a small or compact space and to ensure sufficient natural frequency.

Figure 6 shows the experimental setup consisting of the developed microgripper, piezoelectric driver (MK-V500), data acquisition card (PCI-6221 from NI, Inc.), capacitive displacement sensor (D100 from PI, Inc), piezoelectric actuators, strain sensor, and the computer. The basic operation process of the experimental system is as follows: First, the control signal sent by the computer is applied to the piezoelectric driver through the D/A port of the acquisition card to activate the piezoelectric actuator to produce a certain movement. Changing the control signal can make the microgripper produce various, continuous gripping and releasing movements. Then, the strain gauges glued on the microgripper body can sense the movement of the microgripper, and the strain signal will be transmitted to the computer through A/D port of the acquisition card

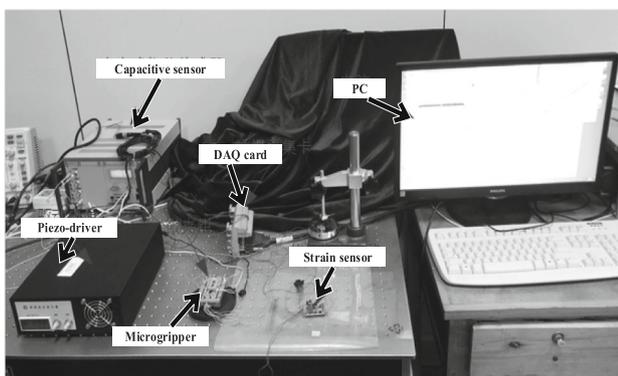


**Fig. 6** Experimental setup

for post-processing. The capacitance displacement sensor is used to calibrate the output signal of strain sensors.

## 4.2 The calibration of sensors

The strain sensor for gripping force measurement is calibrated by using some high-precision weights. The specific implementation steps are as follows: First, place the microgripper side down, and place weights of 1, 2, 5, 10 and 20 gs at the tip of the clamping arm of the microgripper respectively. Then, the gravity of the weights is regarded as the gripping force, and the corresponding voltage value from the strain force sensor was collected. Finally, the calibration coefficient of the strain force sensor can be obtained by fitting the voltage and weight gravity. Figure 7a shows the fitted curve, with correlation coefficient of 0.9980, and then the calibration coefficient of strain force sensor is 0.163 mN/mV.

The strain sensor for measuring the gripping displacement is calibrated by the capacitance displacement sensor. Firstly, a variable driving voltage was applied to the microgripper to make it produce movement, and the electrical signals generated by the strain gauge pasted on the microgripper were recorded. At the same time, capacitance displacement sensor was used to record the output displacement of the clamping arm. Then, the calibration coefficient of the strain displacement sensor can be obtained by comparing the values measured by the two sensors. After that, different driving voltages are used to compare the output curves of the calibrated strain sensor and the standard capacitive sensor. The obtained calibration coefficient can be considered correct if the two curves are in good agreement. Figure 7b shows the measurement results of the two sensors. It can be seen that the displacement curves measured by the calibrated strain sensor are in good agreement with those measured by the standard capacitive sensor. And the corresponding calibration coefficient of the strain displacement sensor is 0.040  $\mu\text{m}/\text{mV}$ .

## 4.3 Characteristic test

In order to test the real displacement amplification ratio of the developed microgripper, a sinusoidal input voltage with 0.1 Hz and 100 Volts, which means a maximum input displacement of 6.10  $\mu\text{m}$ , is applied to the microgripper, and the recorded maximum output displacement is 102.30  $\mu\text{m}$ . Thus, the resulting amplification ratio is 16.8, which can meet the design requirements. A same input voltage is applied to the microgripper when the gripping tip is fixed, we can get the maximum gripping force of 227.70 mN.

Compared with the FEA simulation results, there exists a small error. The reason is that the displacement of the

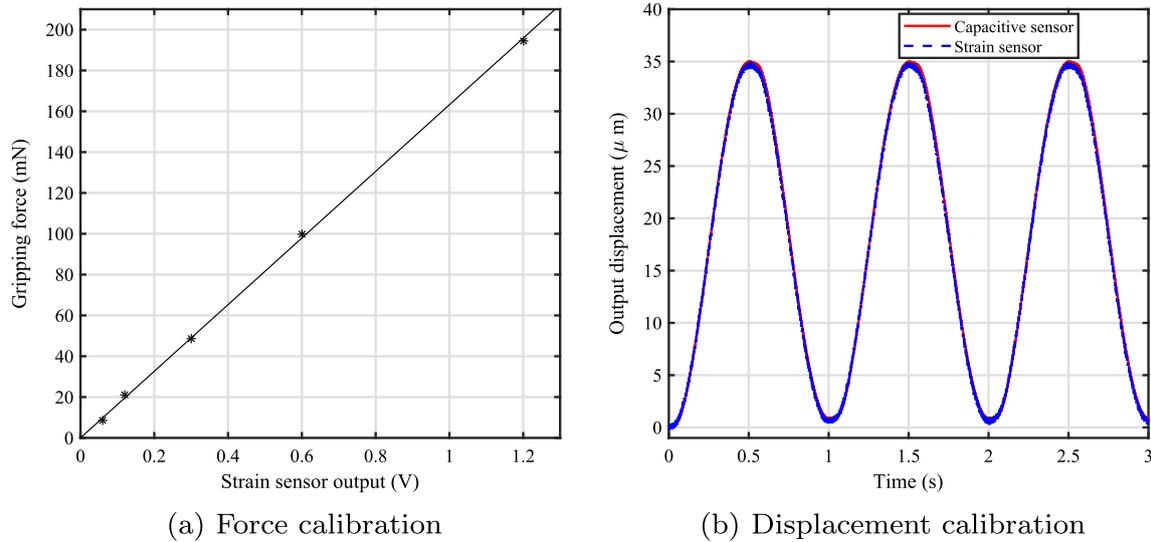


Fig. 7 The calibration of strain sensors

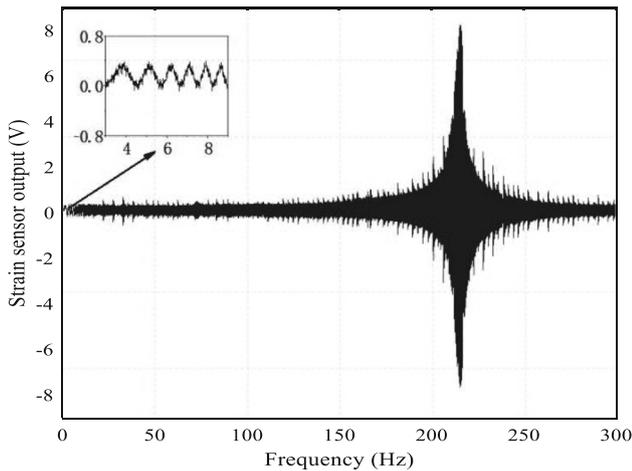


Fig. 8 Response with swept-frequency inputs

piezoelectric actuator is directly used as the input in the simulation, and thus the unconsidered coupling effect between the piezoelectric actuator and mechanical structure produced this small error. It should be noted that, it is normal to have errors between the theoretical, simulated and measured values of the displacement amplification ratio. This is because the theoretical value is a geometrical approximation and material properties were not taken into account, while the simulated value is also an approximation of the actual microgripper and the presence of piezoelectric ceramics was not considered. What we need to make sure is that the final measured displacement amplification ratio is within a reasonable range.

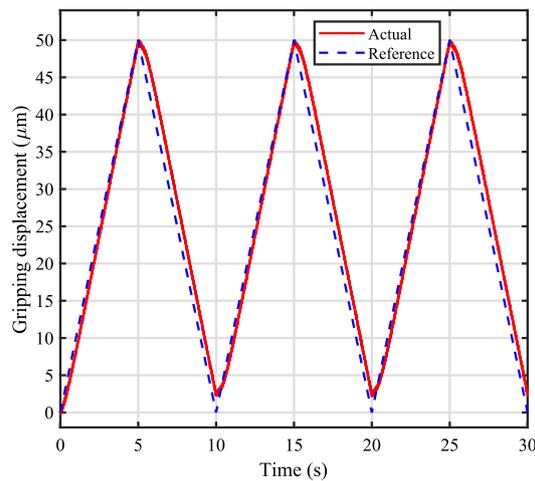
In order to test the resonant frequency of the developed microgripper, a sinusoidal sweep voltage with relatively small amplitude from 0.1 to 300 Hz is applied to the

microgripper, and Fig. 8 shows the recorded output displacements. It can be seen that the first-order natural frequency of the microgripper is about 215.1 Hz, which is smaller than the result of FEA simulation. The reason is that the mass of piezoelectric ceramics is not considered in the FEA simulation.

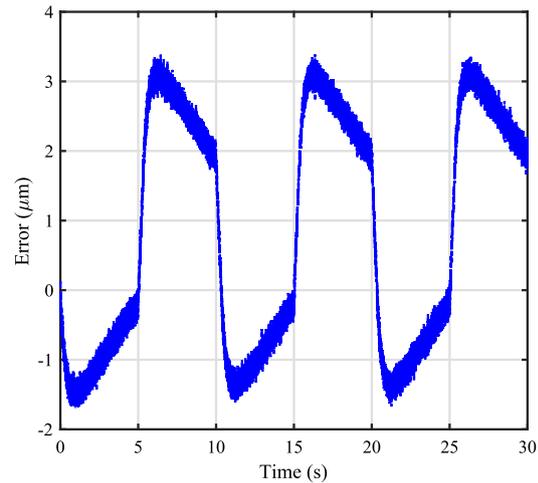
## 5 Experiments

### 5.1 Displacement tracking experiments

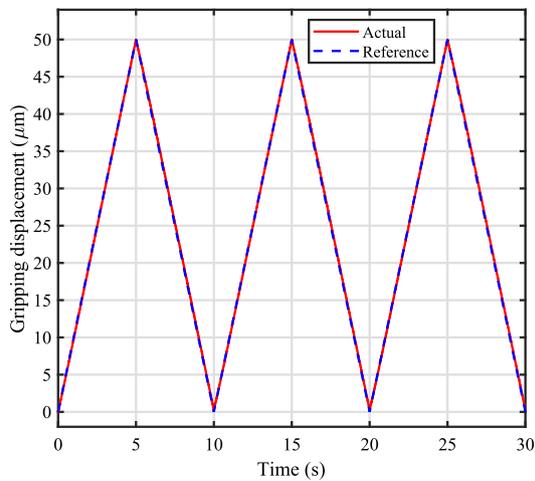
In this subsection, the tracking performance of the motion trajectories of the developed microgripper is explored firstly based on open-loop operation. A periodic triangular voltage with 0.1 Hz, which corresponds to a reference displacement with an amplitude of 50 μm, is applied to the piezoelectric actuator of the microgripper whose displacement responses are recorded accordingly. Figure 9a, b shows the corresponding open-loop experimental results including the reference and real displacements and the errors, which reveals obvious phase lag and displacement error due to the inherent piezoelectric hysteresis and other disturbances. In order to improve the position tracking performance, a proportional-integral (PI) controller is designed to alleviate the tracking error based on closed-loop operation. The constant gains of the PI controller are tuned and finally set as  $k_{1p} = 12$  and  $k_{1i} = 0.3$ . With the same displacement reference commands as the tracking objective trajectories, the obtained real displacement responses and errors of the developed microgripper under the PI control strategy are shown in Fig. 9c, d. The Peak-to-Valley (PV) error of the displacements in open-loop



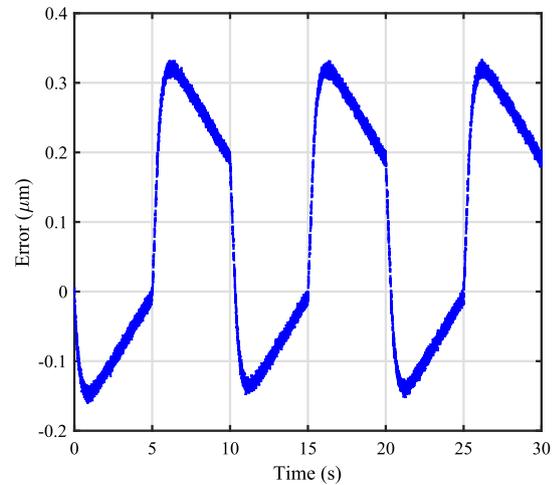
(a) Open loop displacement tracking



(b) Open loop displacement tracking error



(c) Closed loop displacement tracking



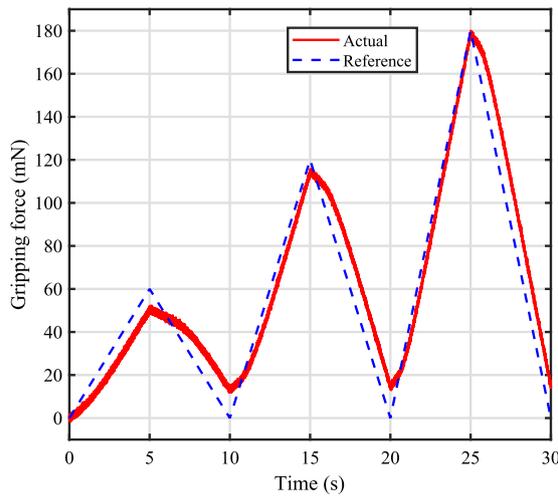
(d) Closed loop displacement tracking error

**Fig. 9** Displacement tracking experiment

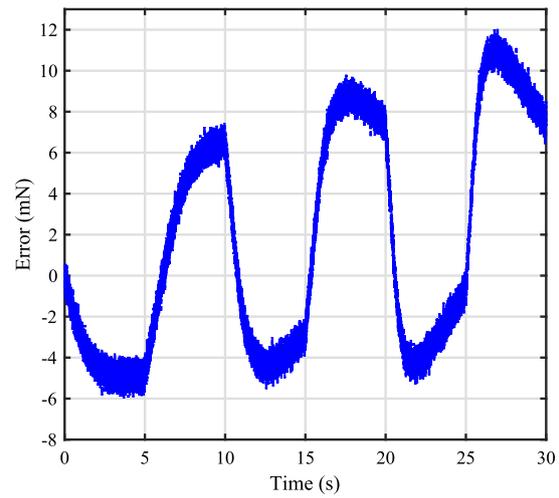
operation is  $5.10 \mu\text{m}$  accounting for 10% of the full tracking range, and the corresponding Root-Mean-Square (RMS) error is  $1.92 \mu\text{m}$ . The PV error of the displacements in closed-loop operation is  $0.49 \mu\text{m}$  accounting for 1% of the full tracking range, and the corresponding RMS error is  $0.19 \mu\text{m}$ . It can be concluded from the above results that (i) the displacement tracking performance of the microgripper under open-loop mode is poor due to the relatively big error and phase lag of position output. (ii) the displacement tracking performance under closed-loop mode is good, because the reference and actual displacements coincide with each other and the position output lag is improved. (iii) the PI controller can effectively eliminate the inherent hysteresis and nonlinearity of the microgripper and realize the precision control of the gripping displacement.

## 5.2 Force tracking experiments

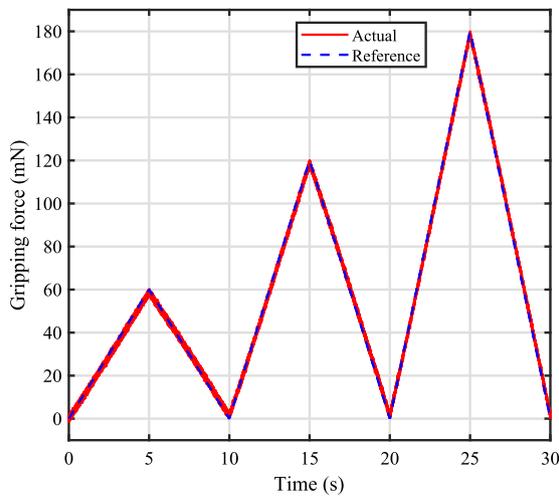
In order to verify the performance of the gripping force, similar force tracking experiments under open and closed loop modes were performed respectively. A varied amplitude triangular voltage command denoting the reference force is applied and then the actual gripping force measured from the force sensor is recorded. Figure 10a, b show the reference force command and the actual force and the errors, respectively. We can see that the PV error of gripping force is  $18.07 \text{ mN}$  accounting for 9% of the full scale range, and the corresponding RMS error is  $5.76 \text{ mN}$ . Obvious phase lag and tracking error can also be found from the results. Similarly, another PI controller was



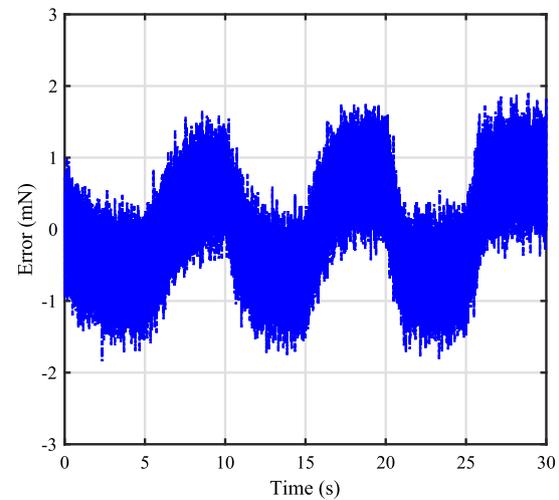
(a) Open loop force tracking



(b) Open loop force tracking error



(c) Closed loop force tracking



(d) Closed loop force tracking error

**Fig. 10** Force tracking experiment

designed in order to improve force tracking performance. The constant gain parameters are set as  $k_{1p} = 25$ , and  $k_{1i} = 0.18$ . Under this closed-loop control strategy and with the same reference force command, the actual gripping force and the corresponding error can be obtained as shown in Fig. 10c, d. The PV error of gripping force in closed-loop operation is 3.74 mN accounting for 2% of the full scale range, and the corresponding RMS error is 0.65 mN. It can be seen that the reference force very coincides with the measured force, deeming that the force tracking performance under closed-loop mode is greatly improved. Thus, the force tracking in closed loop mode can effectively eliminate nonlinearity and control the gripping force effectively and accurately.

### 5.3 Closed-loop gripping experiments

In this subsection, the gripping performance of the microgripper in closed-loop operation mode is verified through the “grasp-hold-release” operation. The experimental curves of force/position switching tracking are shown in Fig. 11. There exist two independent PI control loops in the system. One control loop is used for accurate tracking and monitoring of the displacement, the other one is for precise control and monitoring of gripping force. The specific process of the force/position switching control is as follows:

**Step 1:** (approaching stage) Keep the tracking of displacement, which is divided into fast approaching and slow approaching to reach the gripping object. At the same time, persistently monitoring the holding force. If the gripping

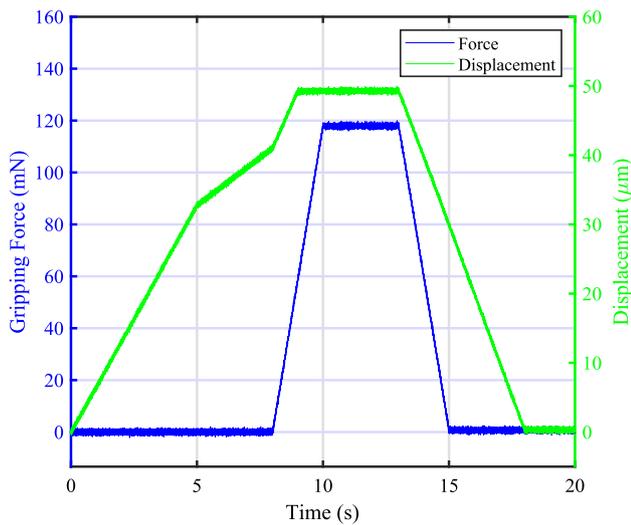


Fig. 11 Closed-loop gripping experiment

force varies from 0 to a small set value, start the force tracking action.

**Step 2:** (holding stage) Keep the tracking of the gripping force, and meanwhile keep monitoring the displacement.

**Step 3:** (releasing stage) Keep the monitoring force and displacement. If the gripping force decreases, and both force and displacement reach zero, terminate the experiment.

#### 5.4 The performance comparison and discussions

The features of the designed piezoelectric microgripper include simple mechanism, compact size, high precision, perceptive force/displacement. The design advantages include: (1) Large clamping range can be achieved by a large displacement amplification ratio through simple structure; (2) High resonant frequency is realized through the compact size, which is conducive to the controller design to achieve large clamping speed; (3) Accurate linearization of clamping force and displacement is realized by closed-loop control-based hysteresis elimination. (4) Translational gripping action can be ensured in principle by the designed symmetrical structure. (5) The simultaneous self-sensing of force and displacement can enhance the clamping performance and avoid the damage of the clamping object.

In the work of Yuguo and Yaoxiang (2015), the largest range of clamping displacement is  $78.35 \mu\text{m}$ , and the holding force is  $9.24 \mu\text{N}$  at a maximum voltage of  $150 \text{ V}$ . In our work, the designed gripper can reach a maximum output displacement of  $102.30 \mu\text{m}$  and the maximum gripping force of  $227.70 \text{ mN}$  at a sinusoidal voltage of  $100 \text{ V}$ . Thus, the designed gripper can reach a larger clamping

range and greater gripping force under a lower driving voltage. This is mainly due to the superiority of the design structure. In the work of Yang et al. (2015), an amplification ratio of 16.4 and a natural frequency of 157.5 Hz are obtained based on a gripper of almost the same size level. In our work, the displacement amplification ratio is 16.8 and the natural frequency is about 215.1 Hz. Thus, the microgripper designed in this paper can achieve faster clamping, because the larger natural frequency is advantageous to achieve better control performance. Compared with the work of Wang et al. (2013), Chen et al. (2019), the two fingers of the microgripper designed in this paper have the ability to move independently, which increases the freedom of motion and control. We can conclude that the designed microgripper has relatively superior performance among similar devices.

It will be helpful for the interested readers to differentiate the basic mechanism of electrostatic and piezoelectric grippers. Electrostatic microgripper is driven by the Coulomb force, and can be divided into parallel-plate type and comb type. This kind of microgripper has the characteristics of small size, simple structure, high precision, so it is widely used in MEMS systems. The piezoelectric microgripper uses the inverse piezoelectric effect to realize the clamping and releasing operation, and it has the advantages of fast response speed, high resolution and large driving force, so piezoelectric microgripper is also widely used. However, the application areas of these two kinds of grippers are different and overlap. Generally speaking, the gripping object of electrostatic microgripper is smaller. For example, literature (Chen et al. 2010) gives a comb type electrostatic microgripper with integrated vacuum pipe. This microgripper realizes the pickup and release of tiny objects through the electrostatic driving force generated by the comb structure and the auxiliary air pressure of the air pump. The microgripper is made by silicon processing, and the vacuum pipe is constructed by bonding technology. Compared with piezoelectric microgripper, the electrostatic microgripper has geometric similarities in mechanical structure, but the manufacturing process has great differences.

## 6 Conclusions

In this paper, a novel three-stage magnification based symmetrical piezoelectric micro-gripper is reported. Firstly, the mechanical structure and working principle are demonstrated. Secondly, the modeling, optimization and analysis for kinematic, static and dynamic characteristics are presented. After that, the sensor calibration for the clamping force and displacement and open and closed-loop performance testing are carefully conducted based on a

series of experiments. The key performance indicators, including amplification ratio of 16.8, clamping range of 102.30  $\mu\text{m}$ , natural frequency of 215.10 Hz, are verified. The design advantages include large clamping range, high resonant frequency, translational gripping action, accurate linearization and simultaneous self-sensing of clamping force and displacement. The designed microgripper has relatively superior performance among similar devices. Our next step will be to further optimize the micro-gripper and to improve its control methods to adapt to different working conditions. How to design the microgripper to achieve a performance balance between static index (stroke) and dynamic index (natural frequency) will also be a future research focus.

**Acknowledgements** This work is supported by the Key Technologies R & D Program of Sichuan Province, China under Grant No. 23ZDYF0471 and by the Doctoral Research Fund of Southwest University of Science and Technology under Grant No. 22zx7140. The authors also thank the anonymous reviewers for their insightful and constructive comments.

**Author Contributions** LN: conceptualization; validation; formal analysis; writing original draft; funding acquisition. GC: investigation; software; analysis; writing revision draft. KH: software; data curation; experiments and testing. GW: conceptualization; methodology; writing- review and editing; funding acquisition. All authors have read and agreed to the final version of the manuscript.

## Declarations

**Conflict of interest** The authors declare that they have no conflict of interests, including any financial and non-financial interests, or personal relationships that could have appeared to influence the work reported in this paper.

## References

- Aabid A, Parveez B, Raheman MA, Ibrahim YE, Anjum A, Hrairi M, Parveen N, Zayan JM (2021) A review of piezoelectric material-based structural control and health monitoring techniques for engineering structures: challenges and opportunities. *Actuators* 10(5)
- Awtar Shorya (2013) Analysis of flexure mechanisms in the intermediate displacement range, chapter 3, pages 27–43. Wiley
- Chang P-L, Chi I-T, Tran Ngoc DK, Wang D-A (2020) Design and modeling of a compliant gripper with parallel movement of jaws. *Mech Mach Theory* 152:103942
- Chen T, Sun L, Chen L, Rong W, Li X (2010) A hybrid-type electrostatically driven microgripper with an integrated vacuum tool. *Sens Actu A: Phys* 158(2):320–327
- Chen W, Zhang X, Li H, Wei J, Fatikow S (2017) Nonlinear analysis and optimal design of a novel piezoelectric-driven compliant microgripper. *Mech Mach Theory* 118:32–52
- Chen X, Deng Z, Siya H, Gao J, Gao X (2019) Design of a flexible piezoelectric microgripper based on combined amplification principles. *Nanotechnol Precis Eng* 2(3):138–143
- Ding B, Yang Z-X, Xiao X, Zhang G (2019) Design of reconfigurable planar micro-positioning stages based on function modules. *IEEE Access* 7:15102–15112
- Fard-Vatan HM, Hamed M (2020) Design, analysis and fabrication of a novel hybrid electrothermal microgripper in microassembly cell. *Microelectron Eng* 231:111374
- Han L, Fang Y, Ren X, Zhang X (2015) Improved direct inverse tracking control of a piezoelectric tube scanner for high-speed afm imaging. *Mechatronics* 31:10
- Jalili B, Aghaee N, Jalili P, Ganji DD (2022) Novel usage of the curved rectangular fin on the heat transfer of a double-pipe heat exchanger with a nanofluid. *Case Stud Therm Eng* 35:102086
- Jalili B, Sadighi S, Jalili P, Ganji DD (2022) Numerical analysis of mhd nanofluid flow and heat transfer in a circular porous medium containing a cassini oval under the influence of the lorentz and buoyancy forces. *Heat Transf* 51(7):6122–6138
- Jalili P, Kazerani K, Jalili B, Ganji DD (2022) Investigation of thermal analysis and pressure drop in non-continuous helical baffle with different helix angles and hybrid nano-particles. *Case Stud Therm Eng* 36:102209
- Koo B-W, Hong S-P, Kim S-I, Kang CS, Han S-S, Oh Kyu H, Kim Young-Woon (2015) Design and application of a novel in situ nano-manipulation stage for transmission electron microscopy. *Microsc Microanal* 21(2):298–306
- Liang C, Wang F, Tian Y, Zhao X, Zhang D (2017) Development of a high speed and precision wire clamp with both position and force regulations. *Robot Comput Integr Manuf* 44:208–217
- Liang C, Wang F, Shi B, Huo Z, Zhou K, Tian Y, Zhang D (2018) Design and control of a novel asymmetrical piezoelectric actuated microgripper for micromanipulation. *Sens Actu A Phys* 269:227–237
- Lyu Z, Qingsong X (2021) Recent design and development of piezoelectric-actuated compliant microgrippers: a review. *Sens Actu A Phys* 331:113002
- Nah SK, Zhong ZW (2007) A microgripper using piezoelectric actuation for micro-object manipulation. *Sens Actu A Phys* 133(1):218–224
- Oden JT, Ripperger EA, Saunders H (1982) *Mechanics of Elastic Structures* (2nd Edition). *J Mech Design* 104(4):681–682
- Paros JM, Weisbord L (1965) How to design flexure hinges. *Mach Des*
- Ren B, Dai J, Zhong Q (2020) Ude-based robust output feedback control with applications to a piezoelectric stage. *IEEE Trans Ind Electron* 67(9):7819–7828
- Wang G, Rao C (2015) Adaptive control of piezoelectric fast steering mirror for high precision tracking application. *Smart Mater Struct* 24(3):035019
- Wang DH, Yang Q, Dong HM (2013) A monolithic compliant piezoelectric-driven microgripper: design, modeling, and testing. *IEEE/ASME Trans Mech* 18(1):138–147
- Wang G, Chen G, Bai F (2015) Modeling and identification of asymmetric bouc-wen hysteresis for piezoelectric actuator via a novel differential evolution algorithm. *Sens Actu A Phys* 235:105–118
- Wang K, Wang D-H, Zhao J-Y, Hou S (2021) A novel piezoelectric-actuated microgripper simultaneously integrated microassembly force, gripping force and jaw-displacement sensors: design, simulation and experimental investigation. *Smart Mater Struct* 31(1):015046
- Wang F, Shi B, Huo Z, Tian Y, Zhang D (2021) Control and dynamic releasing method of a piezoelectric actuated microgripper. *Precis Eng* 68:1–9
- Wang W, Jiang Y, Thomas PJ (2021) Structural design and physical mechanism of axial and radial sandwich resonators with piezoelectric ceramics: a review. *Sensors* 21(4)
- Yang YF, Lei TG, Junqiang L, Yanding W (2015) A bridge-type piezoelectric microgripper with integrated position/force sensors. *Robot* 37(6):655–662

- Yong YK, Tien-Fu L, Handley DC (2008) Review of circular flexure hinge design equations and derivation of empirical formulations. *Precis Eng* 32(2):63–70
- Yuguo LJC, Yaoxiang Z (2015) Detection of finger displacement and gripping force of piezoelectric micro-gripper. *Opt Precis Eng* 23:1372–1379
- Zhang Z, Hu H (2009) Comparison of single-notch circular flexure hinge rotational stiffness equations with fea results and derivation of empirical formulations. In: 2009 International Joint Conference on Computational Sciences and Optimization, volume 1, pages 286–288
- Zhang J, Yang Y, Lou J, Wei Y, Fu L (2018) Development and hybrid position/force control of a dual-drive macro-fiber-composite microgripper. *Sensors* 18(4)
- Zheng L, Weijie D (2022) Position and force self-sensing piezoelectric valve with hysteresis compensation. *J Intell Mater Syst Struct* 33(1):170–182
- Zubir MNM, Shirinzadeh B, Tian Y (2009) A new design of piezoelectric driven compliant-based microgripper for micromanipulation. *Mech Mach Theory* 44(12):2248–2264

**Publisher's Note** Springer Nature remains neutral with regard to jurisdictional claims in published maps and institutional affiliations.

Springer Nature or its licensor (e.g. a society or other partner) holds exclusive rights to this article under a publishing agreement with the author(s) or other rightsholder(s); author self-archiving of the accepted manuscript version of this article is solely governed by the terms of such publishing agreement and applicable law.